4.2 Energy Ramp and Related Effects

One of the important processes that define the stable machine operation with the required beam parameters, the time structure and the efficiency of the beam storage in the main ring is the ramping process in the booster synchrotron. The new larger diameter booster significantly improved the ramping process and reduced the eddy current effects. Its also made it easy to control injection and extraction processes.

 The booster ring magnet system has a separated function lattice that provides for damping of oscillations in all three dimensions: two transverse and longitudinal. Due to the equilibrium beam parameters at the high energy, extraction timing is very flexible in adjusting to the desired operational mode to the storage ring.

4.2.1 RF System

The booster is designed to accelerate the electrons from an injection energy of 100 MeV to full operational energy of 3 GeV with a maximum pulse current of 10 mA and repetition rate of 2 Hz.

The RF system must provide adequate voltage and power to accelerate the beam, to compensate for synchrotron radiation losses while maintaining sufficiently good energy acceptance to achieve a high quality injection beam at full energy. The maximum required accelerating voltage in the booster is basically determined by the energy loss at maximum particle energy and increases as the fourth power of the energy. Because of the large bending radius in the booster dipole magnet of $\rho = 13.75m$, the particle energy loss per turn is only about 0.52 MeV. The comparatively low accelerated beam current of 10 mA (nominal 5 mA) reduces the required RF power supplied to the beam that is at the level of 5.2 kW. The most effective way to achieve beam acceleration is through the usage of a cavity with high shunt impedance thereby minimizing the power loss into the cavity walls and subsequently improving the efficiency of the RF system. The best candidate from this point of view is the normal conducting 6 cells 500 MHz copper DORIS type cavity. The parameters of these cavities are given in Table. 4.2.1.

Table 4.2.1 Parameters of DORIS type multi-cell cavity

Frequency, MHz	499.654
Number of cells	6
Voltage per cell Vcell, (kV)	188
Shunt impedance per cell, Rcell (MΩ)	3
Quality factor Q	28 000

Cavity voltages will be controlled during the acceleration cycle to avoid large particle oscillations in transverse and longitudinal phase spaces at low energy. At the low injection energy of 100MeV, the RF voltage of 250 kV is determined mainly by the RF bucket size (energy acceptance more than 2%) to capture the injected beam with a length of 0.5 ns. Synchrotron radiation loss is dominant at high energies.

The RF system parameters for the booster are given in Table 4.2.2.

Table 4.2.2 Booster RF system parameters.

Beam Energy, E (GeV)	At injection-0.1	At extraction –3
RMS energy spread (%)	-	0.067
RF frequency (MHz)		499.654
Energy acceptance (%)	1.75	0.43
Beam current (mA)	10	10
Energy loss per turn (MeV)	-	0.521
Number of cavities	1	1
Number of cells	6	6
Total RF voltage V_{RF} (MV)	0.3	1.128
Synchronous RF phase (degree)	-	152.49
R.M.S. bunch length (mm)	-	20.07
Synchrotron tune	-	0.01623
Overvoltage factor	-	2.165
Shunt impedance (MΩ)	18 (6 x 3)	18
Power dissipated (kW)	2.5	35.3
RF power into beam (kW)		5.2
Miscellaneous power loss (kW)		10
Total power (kW)		50.5

To achieve zero reflected power in cavity at 3 GeV with full beam loading, the coupling factor $\beta = 1 + P_b / Pw$ can be adjusted to 1.15 and the cavity can be detuned to 2.6 kHz.

4.2.2 Beam Acceleration Performance

The evolution of beam parameters during the acceleration ramp is given by the differential equation

$$\frac{dA}{dt} = -A \cdot (\frac{\dot{E}}{E} + J \cdot \frac{P_\gamma}{E}) + \frac{55}{32\sqrt{3}} \cdot \frac{\hbar \cdot c \cdot \gamma^3 \cdot P_\gamma}{\rho \cdot E^2} \tag{4.2.1}$$

where *A* stands for any of quantities -beam energy spread, bunch length and transverse emittances. For the each of these quantities the second term in right hand side of the equation (4.2.1) must be slightly modified. The first term on the right hand side of the equation describes adiabatic and radiation damping processes while the second term (~ E^5) describes the effect of quantum excitations caused by synchrotron radiation. Intrabeam scattering effects are neglected since they drop strongly with rising beam energy and are very low at the booster injection energy of 100 MeV and current of 10mA.

At the beginning of the ramping process, the beam size, emittance and energy spread are reduced by adiabatic and radiation damping. At an energy of about 1.5 GeV, these parameters reach their minimum value, then quantum effects become important. At the extraction energy they reach their equilibrium values.

The horizontal beam emittance evaluation with energy is shown in Fig. 4.2.1. The initial beam emittance is taken to be 1 mm-mrad. At the low energy part of the ramp the emittance drops due to adiabatic damping and reaches its minimum at an energy of 1.5 GeV. Then, the emittance of the beam is driven basically by the radiation damping and quantum fluctuation effects that lead to an equilibrium beam emittance of 75 nm-rad at the final beam energy of 3 GeV.
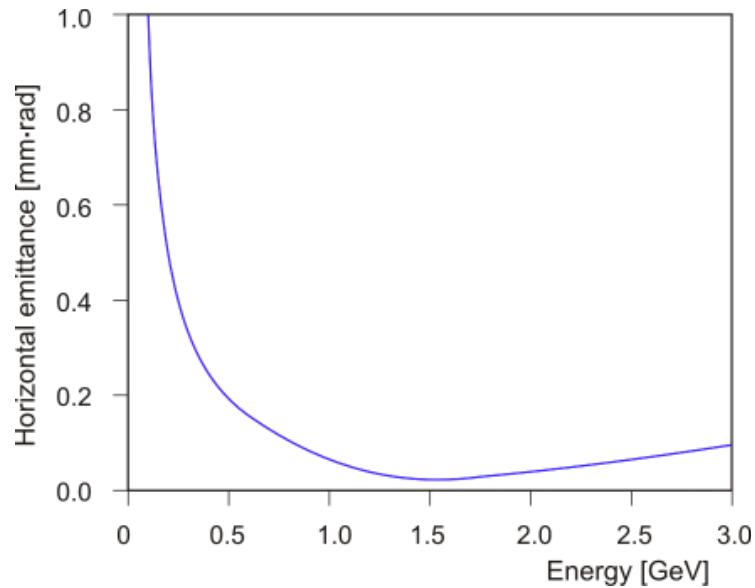
Fig. 4.2.1 Evolution of the beam horizontal emittance during ramping. The minimum emittance of about 30 nm-rad is reached at an energy of 1.5GeV.

The initial time structure of the beam is already bunched at the frequency of 500 MHz at bunching system in linac pre-injector section. Further acceleration of the beam in 3 GHz linac captures the particles in 20 degree of 3 GHz structure. Longitudinal autophasing and the damping of the synchrotron (longitudinal) oscillations in booster synchrotron drive the bunching of the accelerated beam with its rms bunch length reaching its minimum of 5 mm at an energy of about 1.1 GeV (Fig. 4.2.2).

For a RF peak voltage of 1.128MV, the rms bunch length is 20 mm at extraction energy of 3 GeV which comfortably fits into the 500-MHz RF bucket of the storage ring.
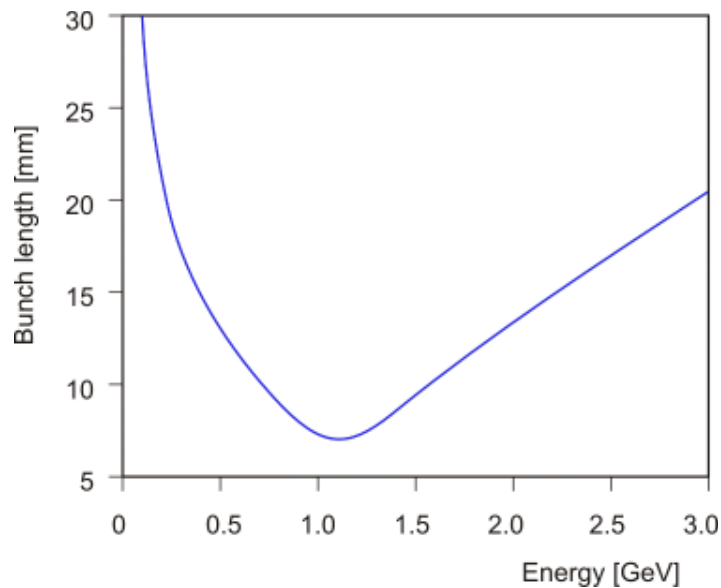
Fig. 4.2.2 Bunch rms length variation during the energy ramp.

The injector linac provides an rms energy spread for the beam of better than 0.5% to minimize beam losses during the injection and first few turns of the beam in the booster. The bunching and radiation related processes that accompany the beam acceleration in the

151

booster shortly after injection drive the rms energy spread within a single bunch. At an energy of about 1.5 GeV the rms energy spread of the beam is stabilized to a level of 0.05% and reaches its equilibrium value of 0.07% at the extraction energy of 3 GeV (Fig 4.2.3).
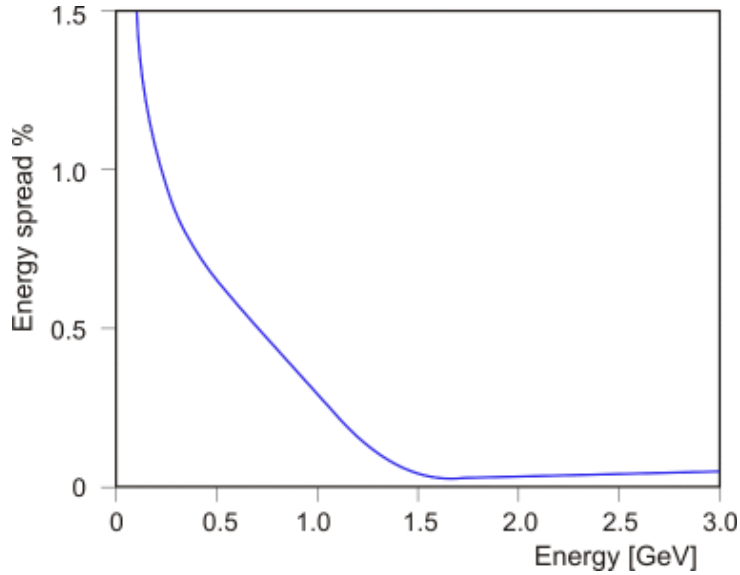
Fig. 4.2.3 Beam rms energy spread variation during acceleration process.

The momentum dependent tunes and betatron functions are plotted in Fig. 4.2.4 and Fig. 4.2.5 respectively. The plots show very stable operation of the beam with an energy spread of $\pm 3\%$. The energy dependent parameters of the booster are summarized in Table 4.2.3.
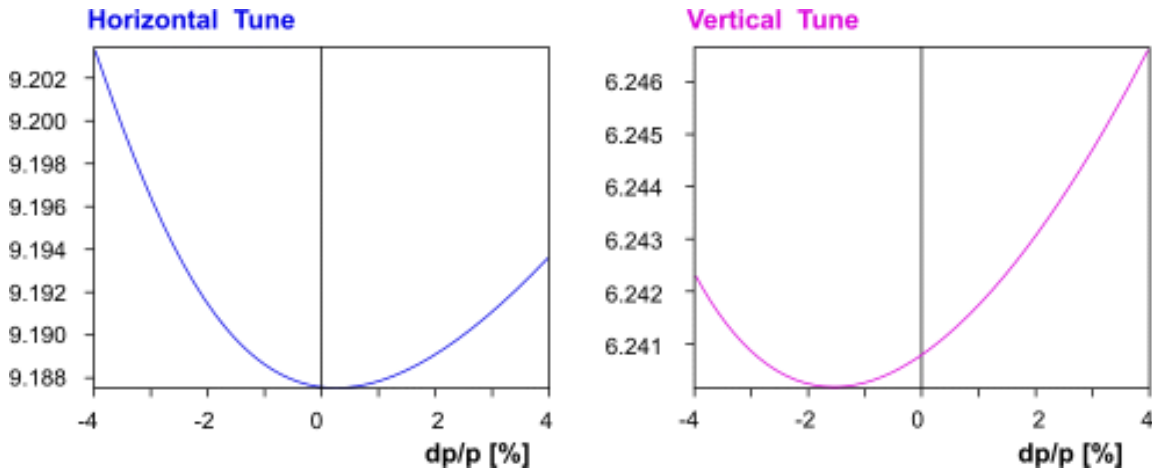
Fig. 4.2.4 Momentum dependent tunes of the booster at extraction energy 3 GeV.
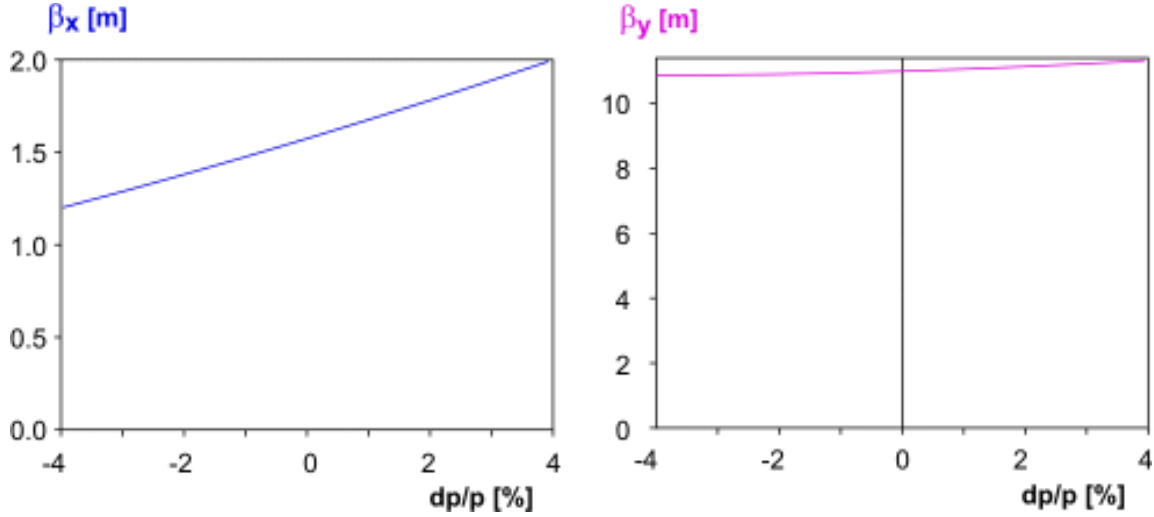
Fig. 4.2.5 Momentum dependence of beta functions at the extraction energy 3 GeV.

**Table 4.2.3 Energy dependent parameters at injection (0.1 GeV)
and extraction (3 GeV) energies.**

Energy (GeV)	0.1	3
Dipole field (T)	0.024	0.723
FQ gradient (T/m)	0.44	13.2
DQ gradient (T/m)	0.36	10.7
FSXT field (T/m^2)	0.012	0.35
DSXT field (T/m^2)	0.016	0.48
Energy loss/turn(KeV)	0.000643	521
Radial damping time (s)	206.43	0.0076
Vertical damping time (s)	199.18	0.0074
Longitud. damping time (s)	97.87	0.0036
RMS energy spread(σ_E / E)%	$2.29\ 10^{-5}$	$6.7\ 10^{-4}$
Radial emittance (nm.rad)	-	74.9
Vertical emittance(nm.rad)	-	0.075

4.2.3 Eddy Current Effects

The time dependent dipolar field of the bending magnets determines the ramping cycle for the booster. For a biased-sine shape time dependent field,

$$B(t) = B_0 \cdot (\alpha - \cos(\omega_0 \cdot t)) \tag{4.2.2}$$

where $\alpha = \dfrac{E_{ext} + E_{inj}}{E_{ext} - E_{inj}}$ and $B_0 = \dfrac{B_{ext}}{\alpha + 1}$, the corresponding energy ramp is:

$$E(t) = E_0 \cdot (\alpha - \cos(\omega_0 \cdot t)) \tag{4.2.3}$$

where $\omega_0 = 2 \cdot \pi \cdot f$ is the ramping frequency.

In the CANDLE booster case $E_{inj} = 0.1 GeV$, $E_{ext} = 3 GeV$, $f = 2 Hz$ and $\alpha \approx 1.07$, $B_0 = 0.351 T$, $E_0 = 1.45 GeV$.

The time dependent fields produce eddy currents in the vacuum chamber of the bending magnet. These currents create a decrease of the magnetic field at the center of the pipe given by:

$$\Delta B = \dot{B} \cdot \frac{\mu_0 k a^2 D}{h} J \qquad (4.2.4)$$

where k is the conductivity of the vacuum chamber, D its thickness and h the magnet half gap. The form factor J is equal to 0.7 for the CANDLE vacuum chamber dimensions. Analysis of this field distortion shows [3] that it can be expressed as a sextupolar time-dependent component given by

$$m = J\mu_0 k \frac{D}{h} \frac{\dot{B}}{B\rho} = J\mu_0 k \omega_0 \frac{D}{\rho h} F(t) \qquad (4.2.5)$$

where $F(t)$ is the relative rate of rise of the dipole field:

$$F(t) = \frac{\dot{B}}{\omega_0 \cdot B} = \frac{\sin(\omega_0 \cdot t)}{\alpha - \cos(\omega_0 \cdot t)} \qquad (4.2.6)$$

The function $F(t)$ and the time dependent beam energy during ramping cycle are plotted in Fig. 4.2.6.

We assume that injection takes place at the start of the ramping and extraction at the end. As show in the plot, the sextupolar contribution will be more important at the start of the ramping cycle. The chromaticity dependence behaves like the function $F(t)$. The maximum value of $F_0(t)$ which occurs at an energy of about 200 MeV can be reduced by a factor of two with the proper choice of the magnet currents second harmonic amplitude and phase.
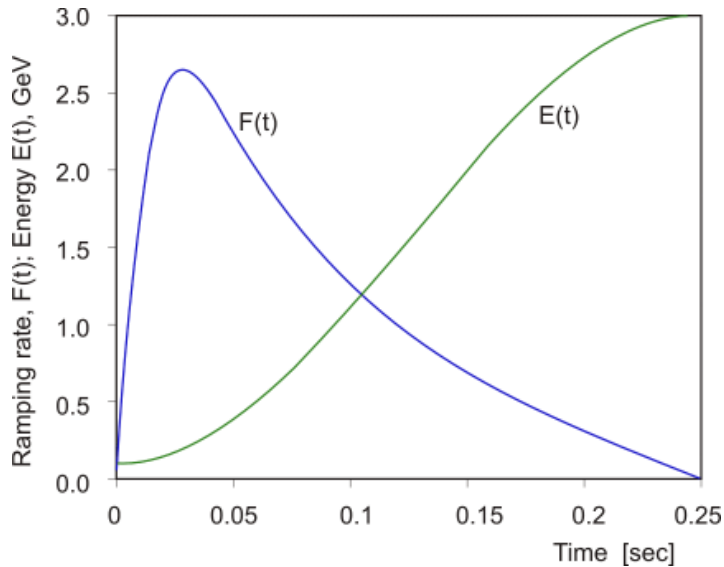
Fig. 4.2.6 Dipole field ramping rate and beam energy variation during the ramp.

The simulation results, including eddy current induced sextupole errors for the repetition rate 2Hz and 3Hz are summarized in Table 4.2.4. To avoid an additional correction of chromaticities during the ramp and to guarantee reliable machine operation we have chosen a repetition rate of 2 Hz.

As one can see from Table 4.2.4 the effect of the eddy currents in the booster is relatively small and no additional sextupoles are needed for sextupolar field compensation.

Table 4.2.4 Eddy current induced sextupole strength in the dipole magnet.

Chamber Material	Stainless steel	
Chamber thickness (mm)	0.7	0.7
Chamber Aperture (mm x mm)	30x20	30x20
Magnet gap height (mm)	30	30
Repetition rate, f_0 (Hz)	2	3
Field rise rate, $F_0(t)$	2.65	2.73
Max sext. strength (m^{-3})	0.07	0.11

The effect of eddy currents upon the quadrupole field can be estimate by the formula:

$$\frac{\Delta g}{g} \approx -\frac{7}{16}\mu_0 kD\, r\, \frac{\dot{B}}{B} \qquad (4.2.7)$$

This change of quadrupole gradient brings a shift to the betatron tunes given by:

$$\frac{\Delta Q}{Q} = \frac{\beta K}{4\pi Q}\frac{\Delta g}{g} \qquad (4.2.8)$$

where r is the average radius of the pipe, $K = \dfrac{gl}{B\rho}$, g -is the quadrupole field gradient and, l is the quadrupole length. For the parameters of the CANDLE booster this change of tunes is negligible small $\dfrac{\Delta Q}{Q} \approx -1.2\cdot 10^{-3}$.

References

1. Yu. Martirosyan, B.Grigoryan and V.Tsakanov, Booster Synchrotron for CANDLE Light Source, Proc. SSILS, Shanghai, China, Sep.2001
2. SLS Handbook, 1999.
3. G. Hemmie, J. Rosbach, Eddy Current Effects in the DESYII Dipole Vacuum Chamber, DESY